Coupled experimental and DFT + U investigation of positron lifetimes in UO_2

Julia Wiktor,[1,*] Marie-France Barthe,[2] Gérald Jomard,[1] Marc Torrent,[3] Michel Freyss,[1] and Marjorie Bertolus[1]
[1]*CEA, DEN, DEC, Centre de Cadarache, 13108, Saint-Paul-lez-Durance, France*
[2]*CNRS/CEMHTI, CNRS UPR 3079/CEMHTI, 45071 Orléans, France*
[3]*CEA, DAM, DIF, F-91297, Arpajon, France*
(Received 27 May 2014; revised manuscript received 20 October 2014; published 4 November 2014)

We performed positron annihilation spectroscopy measurements on uranium dioxide irradiated with 45 MeV α particles. The positron lifetime was measured as a function of the temperature in the 15–300 K range. The experimental results were combined with electronic structure calculations of positron lifetimes of vacancies and vacancy clusters in UO_2. Neutral and charged defects consisting of from one to six vacancies were studied computationally using the DFT + U method to take into account strong correlations between the 5f electrons of uranium. The two-component density functional theory with two different fully self-consistent schemes was used to calculate the positron lifetimes. All defects were relaxed taking into account the forces due to the creation of defects and the positron localized in the vacancy. The interpretation of the experimental observations in the light of the DFT + U results and the positron trapping model indicates that neutral $V_U + 2V_O$ trivacancies (bound Schottky defects) are the predominant defects detected in the 45 MeV α irradiated UO_2 samples. Our results show that the coupling of a precise experimental work and calculations using carefully chosen assumptions is an effective method to bring further insight into the subject of irradiation induced defects in UO_2.

DOI: 10.1103/PhysRevB.90.184101 PACS number(s): 78.70.Bj, 61.72.jd, 71.15.Mb

I. INTRODUCTION

Uranium dioxide is currently the most widely used fuel material in fission reactors. During reactor operation, the fission of uranium atoms causes the formation of defects, such as vacancies and vacancy clusters, as well as the creation of fission products, which induce a significant evolution of the fuel physical properties. The vacancies can trap insoluble fission products, in particular fission gases and it is of great importance to understand their role in the early stages of the formation of gas bubbles in UO_2. Separate effect experiments and atomic scale modeling can bring invaluable insight into the elementary mechanisms involved. The necessity of an improved understanding of the fuel behavior under irradiation has already led to extensive experimental [1–12] and theoretical studies on point defects [13–23] in UO_2.

One of the experimental techniques permitting the investigation of vacancy defects created by irradiation is positron annihilation spectroscopy (PAS). PAS is a nondestructive experimental method that allows studying open volume defects in solids. Vacancies can trap positrons, what is seen through, e.g., changes in the lifetime of positrons in the material. To identify the types of defects present in the examined materials, however, comparison with calculated positron lifetimes or with results of other characterization techniques is required. PAS allows one to detect neutral and negative defects only, since positive ones have a positron trapping coefficient too small to be observed. Moreover, the neutral and negative defects can be distinguished, as the trapping coefficient of negative vacancies decreases with temperature while it is constant for neutral defects [24].

Experimentally, several PAS measurements of the positron momentum distribution (Doppler broadening) [6–11] and positron lifetimes [8,12] have been performed in UO_2. No calculations, however, are available to help in the interpretation of the results of these experiments and in the identification of the defects present in the samples. We present here the results of additional positron lifetime measurements as a function of temperature, as well as the calculations of positron lifetimes in the two-component density functional theory (TCDFT) [25]. Since standard DFT fails to describe the strong correlations between the 5f electrons of uranium in UO_2, we applied the DFT + U method [26] to compute the electron structure of the system. We use self-consistent positron lifetime calculation schemes and we take into account the defects relaxations, since it has been shown that this effect can strongly affect the calculation results in semiconductors and insulators [27–34].

This article is organized as follows. In Sec. II, we describe experimental details concerning the samples characteristics, the irradiation conditions, as well as previous analyzes and present PAS measurements. We also present briefly the positron trapping model used for experimental data analysis. In Sec. III, we describe the methods used in the calculations of positron lifetimes and we list the computational details. In Sec. IV, we show the results of the PAS measurements in the α irradiated samples. In Sec. V, we present the results of the positron lifetime calculations in UO_2. Finally, in Sec. VI, we combine the results of experiments and calculations to discuss the nature of the defects created in the samples. Additionally, we compare our calculations results with the experimental positron lifetimes observed in UO_2 reported in the literature.

II. EXPERIMENTAL DETAILS

A. Samples

The sintered disks of uranium dioxide (0.2 at.% ^{235}U) were polished and were then annealed for 24 hours at 1700 °C under Ar/H_2 atmosphere containing an appropriate amount of water vapor to preserve their stoichiometric composition. The mean grain size was about 18 μm and the mean O/U ratio

*julia.wiktor@cea.fr

was 2.0051 ± 0.0001 as determined by polarography. The density of the material was 10.76 ± 0.03 g cm^{-3}. The disks were 300 − μm thick and 8.2 mm in diameter.

B. Irradiation

The UO_2 disks were irradiated with 45 MeV α particles at a fluence of 2 × 10^{16} cm^{-2} at 300 K. The damaged layer thickness that can be induced by these particles in UO_2 is 347 μm, which is more than the thickness of the sample.

C. Previous PAS analyzes

The same samples were already studied by positron annihilation spectroscopy at room temperature in a previous work [8]. A positron lifetime of 169 ± 1 ps was measured in polished and annealed samples. This value can be attributed to the positron lattice lifetime of UO_2, which corresponds to the case when all positrons annihilate in the free state without being trapped. The samples were then irradiated with electrons and α particles with different energies at various fluences.

No defect was detected after irradiation with 1 MeV electrons. Considering the accepted O and U thresholds displacement energy of respectively 20 and 40 eV [35], this type of irradiation should create defects in the oxygen sublattice only. The oxygen vacancies are predicted to have a positive charge state [14,21,22] in UO_2 close to the stoichiometry, hence cannot be detected by the positrons. This is consistent with the fact that no defect was seen in PAS.

After irradiation of the UO_2 disks with 2.5-MeV electrons and 45-MeV α particles, positron long-lifetime components between 301 ± 7 and 307 ± 3 ps were detected. Based on the U threshold displacement energy, these components were attributed to a defect involving the uranium displacement, such as the U monovacancy, the U-O divacancy or the bound Schottky defect. In this earlier study, however, the measurements on irradiated samples were performed at room temperature only, hence no further information about the charge states of the observed defects could be accessed. Additionally, it is worth noting that the error bars presented in the previous study (from ±3 to ±7 ps) correspond to the statistical accuracy of the fit performed to obtain the lifetime spectra decomposition and not to the actual accuracy of the measurement. Therefore, considering a range of positron lifetimes of 300 ± 10 − 310 ± 5 ps for the previous study would be more reasonable.

D. Present PAS measurements

In the present study, positron lifetime measurements were performed as a function of temperature in the 15–300 K range. A conventional fast-fast coincidence spectrometer with a time resolution of 230 ps was used. A ^{22}Na positron source was sandwiched between two identical samples. Approximately two million events were collected for each spectrum. The lifetime spectra can be expressed as

$$L(t) = R(t) * \sum_i I_i \exp\left(\frac{-t}{\tau_i}\right) + BG, \quad (1)$$

where R is the Gaussian resolution function of the spectrometer and BG the background signal. The spectra were analyzed using a modified version of the POSFIT [36] software. After source and background substraction, the data were fitted to a sum of exponential lifetime components τ_i weighted by the intensities I_i convoluted with a Gaussian resolution function R, giving

$$R(t) * \sum_i I_i \exp\left(\frac{-t}{\tau_i}\right). \quad (2)$$

Theoretical average positron lifetime can be calculated as $\tau_{\text{av.}} = \sum_i I_i \tau_i$.

E. Positron trapping model

The evolution of the positron annihilation characteristics as a function of the measurement temperature can be analyzed using a positron trapping model, which has already been described and applied in various studies [37–44]. In this model, the description of the positron trapping and annihilation at different states (in the free state in the lattice and in N different defects) is obtained through solving a set of rate equations [31]:

$$\frac{dn_{\text{L}}}{dt} = -\left(\lambda_{\text{L}} + \sum_j \kappa_j\right) n_{\text{L}} + \sum_j \delta_j n_{\text{D}j}, \quad (3)$$

$$\frac{dn_{\text{D}j}}{dt} = \kappa_j n_{\text{L}} - (\lambda_{\text{D}j} + \delta_j) n_{\text{D}j} \ (j = 1, \ldots, N), \quad (4)$$

where n_{L} is the probability of a positron being in the free state, $n_{\text{D}j}$ is the probability of being trapped in a given defect. λ_{L}, $\lambda_{\text{D}j}$, κ_j and δ_j are annihilation, trapping and detrapping rates, respectively. The trapping rate is related to the defect concentration c_j through the relation $\kappa_j = \mu_{\text{D}j} c_{\text{D}j}$, where $\mu_{\text{D}j}$ is the specific trapping coefficient. For neutral defects, $\mu_{\text{D}j}$ is temperature independent, while for negative vacancies it varies as $T^{-1/2}$. A positron can be trapped not only in open volume defects, but also by hydrogenlike Rydberg states around negative nonvacancy defects, caused by the long-range Coulomb potential. The positron trapping rate at the Rydberg states also varies as $T^{-1/2}$ [41].

III. CALCULATION METHODS

A. Positron lifetime calculations

To calculate the positron lifetime, it is necessary to know the distributions of both the positron density $n^+(\mathbf{r})$ and the electron density $n(\mathbf{r})$ in the system, as they determine the probability of annihilation. The positron lifetime τ depends on this probability and can be calculated as an inverse of the trapping rate λ:

$$\frac{1}{\tau} = \lambda = \pi c r_0^2 \int_{\mathbb{R}^3} \mathrm{d}^3\mathbf{r}\, n^+(\mathbf{r}) n(\mathbf{r}) g(n^+, n), \quad (5)$$

where c is the light velocity and r_0 is the classical radius of an electron. The $g(n^+,n)$ term is an enhancement factor taking into account the increase in the electron density at the positron site caused by the screening of this particle by electrons.

Positron and electron densities, needed for the positron lifetime calculation, can be computed using a self-consistent scheme, in the two component density functional theory (TCDFT) [25]. Several calculation methods using different

parametrization and approximations exist [45–47]. In this study we use two methods, one proposed by Giglien, Galli, Gygi, and Car (GGGC) [45] and one based on Boroński and Nieminen [46] calculation method, with a parametrization by Puska, Seitsonen, and Nieminen (PSN) [47]. Both these methods are described in Ref. [47] and we will recall here only their main features.

In both GGGC and PSN schemes, several self-consistent computation steps are performed. First, the electron density is calculated, then the density of a positron interacting with the electrons. Later, the electron density affected by the positron is recalculated and then these steps are repeated until convergence is reached. The two self-consistent schemes use, however, different approximations and parametrizations. The GGGC scheme uses the LDA electron-positron correlation functional parametrized for the positron density tending to zero (zero-positron-density limit). This functional was parametrized by Boroński and Nieminen [46] using the data provided by Arponen and Pajanne [48]. For the enhancement factor g, the form depending only on the electron density, modeled by Boroński and Nieminen, is taken [46]. In the PSN scheme, a full LDA electron-positron correlation functional provided by Puska, Seitsonen, and Nieminen [47] is used. The enhancement factor in this scheme depends on both the electron and the positron densities. Since the PSN scheme uses a full electron-positron correlation functional it is more suitable for describing localized positrons, e.g., trapped in defects. The GGGC scheme, on the other hand, tends to overestimate the positron localization [45,47].

The enhancement factor g in Eq. (5) is used in order to take into account the increase in the electron density at a positron site due to the screening of the positron by electrons. However, most of the positron calculation schemes were developed to model metallic materials and they assume a perfect screening of the positron by the electrons. In semiconductors and insulators, corrections have to be used to take into account the existence of the gap in the electronic states. Two types of corrections are available. A semiconductor correction (SC) can be implemented in the enhancement factor as proposed by Puska [49]. Alternatively, a gradient correction (GC) proposed by Barbiellini *et al.* [50] can be implemented in both the enhancement factor and the electron-positron correlation energy.

It is worth noting that the semiconductor correction has already been implemented in both GGGC and PSN schemes [32,49], while the gradient correction existed only in the GGGC method. For the purposes of this study, we decided to implement the gradient correction in the PSN method. Firstly, we implemented the correction, taking an adjustable parameter $\alpha = 0.22$, as proposed by Barbiellini *et al.* [50], in both the enhancement factor g and the correlation energy. However, it is worth noting that this correction was adapted to the LDA zero-positron-density limit. Our implementation of the gradient correction in the correlation energy in the PSN method led to some instabilities in the convergence cycle. Since the correction proposed by Barbiellini *et al.* was intended for a simpler formulation of the correlation functional than the one used in the PSN scheme, we suppose that the latter requires a more complex approach. Both Barbiellini *et al.* in Ref. [50] and Kuriplach *et al.* in their recent work [51] showed that the gradient correction has a significant influence on the enhancement factor while the positron density remains almost unaffected. We decided, therefore, to apply the gradient correction on the g function only in the PSN scheme, by taking

$$g_{\mathrm{GGA}}^{\mathrm{PSN}} = 1 + \left(g_{\mathrm{LDA}}^{\mathrm{PSN}} - 1\right)e^{-\alpha\epsilon}, \tag{6}$$

where ϵ is a parameter, $\epsilon = |\nabla \ln n|^2/q_{\mathrm{TF}}^2$, with $1/q_{\mathrm{TF}}^2$ being the local Thomas-Fermi screening length.

We test in Sec. III C the influence of the choice of the self-consistent scheme and the correction applied to the enhancement factor g on the calculated lattice positron lifetimes (lifetimes obtained in perfect UO_2 cells).

It has been shown for several materials [27–34] that atomic relaxation effects influence strongly the positron lifetimes. Therefore, to consider a full relaxation of defects, the forces on atoms due to the positron, electrons and other nuclei were calculated using the Hellman-Feynman theorem after convergence on both the electronic and positronic densities was reached. By doing this, we obtained exact forces including all the contributions from the positron and the electrons and did not need to add extra Pulay forces as was done in several TCDFT implementations.

B. Computational details

Calculations presented in this paper were performed using the ABINIT [52,53] code, which uses pseudopotentials and a plane-wave basis set or projector augmented-wave [54] (PAW) method for the wave function representation. We used the PAW method available in the code. The TCDFT was implemented previously as a double loop on the electronic and positronic densities: during each subloop, one of the two densities was kept constant while the other was being converged. The TCDFT method has been implemented in ABINIT in an unified formalism for the positron and the electrons: the wave functions of the electrons and the positron in the system are expressed on the same mixed basis (plane waves and atomic orbitals). The atomic orbital basis must be built with care in order to be sufficiently complete to represent the positronic and electronic wave functions with the same accuracy. This issue can be solved by generating atomic data sets with additional basis functions and including semicore states, as described in Ref. [32]. The atomic data sets used in the present study were generated by the ATOMPAW code [55]. The generalized gradient approximation (GGA) as parametrized by Perdew, Burke, and Ernzerhof (PBE) [56] was used to describe the exchange-correlation interactions. Moreover, a Hubbard-like term (U) was added in order to take into account the strong correlations between the $5f$ electrons of the uranium atoms. The Liechtenstein scheme [57] of the DFT + U method was used. The values of the U and J parameters were set to 4.5 and 0.51 eV respectively, in agreement with earlier DFT + U calculations [26] and the values extracted from experiments [58]. To avoid the convergence to one of the metastable states yielded by the DFT + U method and ensure that the ground state was reached, we used the occupation matrix control scheme [17].

For calculations of the defects lifetimes, we used supercells containing 96 atomic sites ($2 \times 2 \times 2$ repetitions of the fluorite unit cell) and $2 \times 2 \times 2$ Monkhorst-Pack **k**-point meshes [59]. We performed calculations for oxygen and uranium monovacancies (V_O and V_U), U-O and U-U

divacancies ($V_U + V_O$ and $2V_U$), a trivacancy containing one uranium vacancy and two oxygen vacancies ($V_U + 2V_O$), a $2V_U + 2V_O$ tetravacancy, and a $2V_U + 4V_0$ hexavacancy. For all clusters, the vacancies were considered as first neighbors. In the case of the $V_U + 2V_O$ trivacancy, also known as the bound Schottky defect, we considered the three possible configurations, with the two oxygen vacancies aligned along (100), (110), and (111) directions. We calculated the positron lifetimes for neutral and charged defects. In the case of the neutral defects, we removed certain atoms to create vacancies. To obtain charged defects, we further added or removed a given number of electrons in the supercell (e.g., we removed one uranium atom and added four electrons to obtain the V_U^{4-} vacancy). We verified that the additional charges were localized at the defect site. Defect charges for which the formal charge of uranium and oxygen ions in UO_2 (O^{2-} and U^{4+}) is conserved were considered since it was shown that these charges are the most stable ones for Fermi levels close to the middle of the band gap [14,21,22]. We did not take into account the spin-orbit coupling because of the high computational cost. Extensive investigations of the SOC influence on the properties of actinide compounds [60,61] suggest that it does not affect the properties of defects [62].

We use a Gaussian smearing of 0.1 eV and a plane-wave cutoff energy of 500 eV. We perform positron lifetime calculations at the equilibrium volume of UO_2 found using the GGA + U method, which was chosen based on the results of the tests described in Sec. III C. We fix the lattice parameters to $a = b = 5.57$ Å and $c = 5.49$ Å for perfect UO_2. The distortion in the z axis is due to the approximate $1\mathbf{k}$ antiferromagnetic order. Atomic relaxation was taken into account and calculations were stopped when the forces acting on atoms were smaller than 0.03 eV/Å, which was found to be sufficient to have the positron lifetime converged with a precision of less than 1 ps.

C. Tests of the parameters used in positron lifetime calculations

We studied the effect of the parameters used in the calculations on the positron lifetime of perfect UO_2. We compared the results obtained in GGA and GGA + U methods, while (1) using different cell volumes, (2) taking two types of positron lifetime calculation schemes, (3) applying different corrections to the enhancement factor g, and (4) considering or neglecting the spin polarization.

Results of these tests are presented in Table I. We used two different calculation schemes, PSN and GGGC (see Sec. III A). GGGC + SC and PSN + SC in Table I refer to schemes in which the semiconductor correction, based on the one proposed by Puska [49] and described in Ref. [32], was implemented. We took the experimental high-frequency dielectric constant of UO_2 of 5.1 [63] in the semiconductor correction. GGGC + GC and PSN + GC refer to schemes in which the gradient correction, proposed by Barbiellini *et al.* [50], was implemented. It is worth noting that in the GGGC + GC scheme this correction is applied on both the enhancement factor and the electron-positron correlation functional, while in the PSN + GC method it is only implemented in the enhancement factor g, as described in Sec. III A. In Table I, we present the lattice positron lifetimes calculated using different volumes. $V^{\text{exp.}}$ refers to the experimental volume, corresponding to a lattice parameter of 5.47 Å [64]. $V^{\text{eq.}}$ refers to the equilibrium volume found in calculations using given parameters. We can notice that the lifetimes obtained using the semiconductor correction, both using the PSN and GGGC schemes, are systematically shorter than the ones calculated with the gradient correction. Moreover, the GGGC and PSN schemes yield similar lattice positron lifetimes, both when the semiconductor and the gradient correction is used. Additionally, the results obtained using the gradient correction are in better agreement with the experimental lattice lifetimes obtained for UO_2 of 169 ± 1ps [8]. It suggests that the schemes using the gradient correction are more suitable for the description of positron lifetimes in uranium dioxide, hence we choose to use them in the present study. We decide to use both GGGC + GC and PSN + GC schemes in our further study of defects positron lifetimes. First, we do it in order to avoid the misinterpretation of experimental results, that could result from possible errors of one of the calculation methods. Second, since the studies in which different self-consistent schemes are used are scarce, we wish to compare those two methods and verify the influence of the scheme choice on the defects identification.

In Table I we can also observe that in each scheme, when the experimental volume is considered, we obtain similar results while using different descriptions of the electrons in the system. No effect of the functional used for the electron-electron exchange-correlation functional description or of the spin polarization is observed. In particular, it is worth noting that the U parameter does not affect directly the calculated positron lifetimes. The difference between the lifetimes calculated in GGA and GGA + U methods is of 1 ps at most, when the experimental volumes are taken. The lifetimes calculated at the equilibrium volumes found using given method, however, differ more strongly. This is because positron lifetime is highly sensitive to the free volume. The best agreement between the calculated and experimental lifetime is

TABLE I. Lattice positron lifetime of UO_2 calculated using various computational parameters.

	GGA				GGA + U			
	no spin		spin		no spin		spin	
	$V^{\text{eq.}}$	$V^{\text{exp.}}$	$V^{\text{eq.}}$	$V^{\text{exp.}}$	$V^{\text{eq.}}$	$V^{\text{exp.}}$	$V^{\text{eq.}}$	$V^{\text{exp.}}$
PSN + SC	151 ps	157 ps	155 ps	157 ps	152 ps	157 ps	160 ps	156 ps
GGGC + SC	149 ps	155 ps	150 ps	154 ps	154 ps	155 ps	158 ps	154 ps
PSN + GC	156 ps	162 ps	161 ps	162 ps	158 ps	162 ps	167 ps	162 ps
GGGC + GC	157 ps	164 ps	159 ps	164 ps	163 ps	164 ps	168 ps	163 ps

reached for the calculation using the GGA + U method and spin polarization at the equilibrium volume (168 and 167 ps in the GGGC + GC and PSN + GC schemes, respectively, compared to 169 ± 1ps measured experimentally). This is, therefore, the set of parameters that we use further in this study.

IV. EXPERIMENTAL RESULTS

The evolution of the annihilation characteristics as a function of the measurement temperature in 45 MeV α irradiated UO_2 disks is presented in Fig. 1. For all measurement temperatures two positron lifetimes are extracted from the experimental spectrum decomposition. The shortlifetime component τ_1, the long-lifetime component τ_2, the average positron lifetime $\tau_{av.}$ and the intensity I_2 corresponding to τ_2 are represented in Fig. 1.

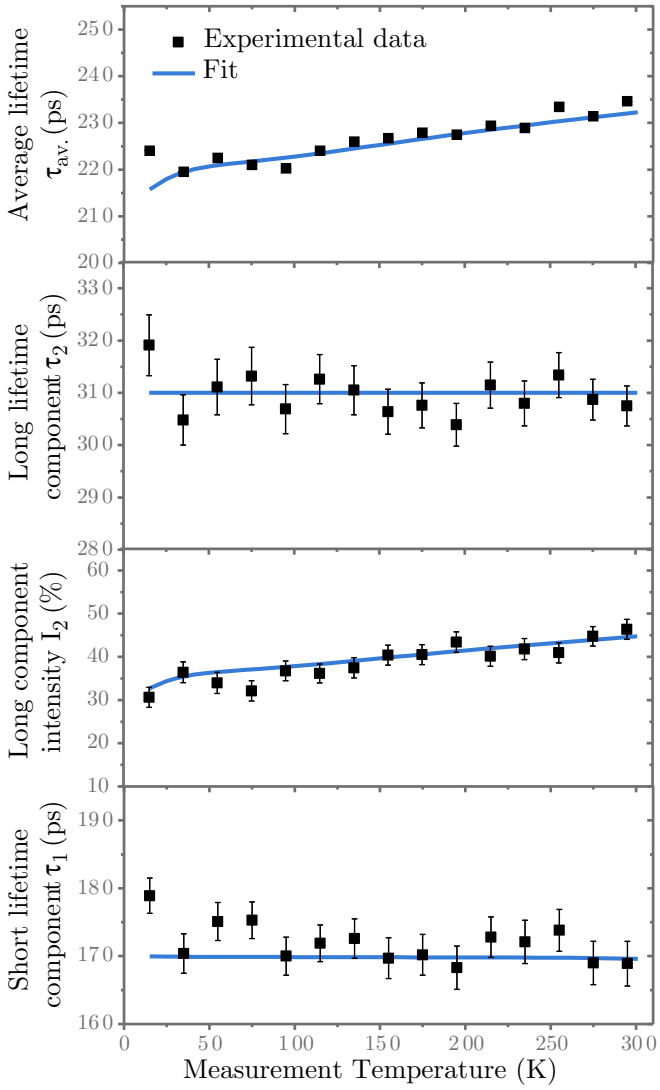

FIG. 1. (Color online) Evolution of the average positron lifetime $\tau_{av.}$, short- and long-lifetime components τ_1 and τ_2 and the intensity I_2, detected in UO_2 crystals irradiated with 45 MeV α particles at a fluence of 2×10^{16} cm^{-2}, as a function of the measurement temperature. The solid lines are the fits to the experimental data obtained from the positron trapping model.

It can be seen that $\tau_{av.}$ increases slightly from approximately 220 ± 5 to 235 ± 5 ps when the temperature rises, while τ_1 and τ_2 remain stable at about 170 ± 5 and 310 ± 5 ps, respectively. The I_2 intensity increases when the measurement temperature rises, similarly to the average positron lifetime $\tau_{av.}$

For all measurement temperatures, the values of τ_2 are much larger than the lattice lifetime, already determined in unirradiated UO_2 disks [8] (169 ± 1ps). This indicates positron trapping in vacancy defects. In addition, the short-lifetime component τ_1 remains close to the experimental lattice lifetime of UO_2. In the case of materials containing only vacancy defects, if some of the positrons had annihilated in a delocalized state (in the lattice), the short-lifetime component would have been shorter than the perfect lattice lifetime since the average time spent by the positron in the lattice would be shorter due to trapping in the defects. Thus the values of τ_1 indicate that all the positrons were trapped in vacancies or in negative nonvacancy defects. The short-lifetime component is still equal to the experimental lattice lifetime at 300 K, which means that the nonvacancy traps are still effective at this temperature. The nature of these nonvacancy defects will be discussed further in Sec. VI.

The long-lifetime component τ_2 changes only slightly as a function of measurement temperature and remains stable at 310 ± 5 ps. This positron lifetime is close to the positron long-lifetime components ranging from 300 ± 10 to 310 ± 5 ps observed in the previous study on the same samples [8] and 313 ± 19 ps detected in UO_2 with 0.2% plutonium weight content [12]. The intensity I_2 corresponding to the long-lifetime component increases slightly when temperature rises, which means that its trapping rate changes only slightly.

To determine the nature of the vacancy-type defects detected in the samples, we used a positron trapping model (see Sec. II E). First, we considered models with only two types of positron traps (negative nonvacancy defects and neutral or negative vacancies). Both of them, however, failed to reproduce the experimental data. We concluded, therefore, that at least three types of traps were present in the studied samples—negative nonvacancy defects, neutral, and negative vacancies—and that the corresponding model should be used. The solutions of the rate equations used in the model containing three different defect types were obtained by Krause-Rehberg and Leipner [41].

The fits to the experimental data obtained using the positron trapping model are presented in Fig. 1 (solid lines). Several parameters are needed in the model, some of which must be deduced or estimated. For the lattice and the nonvacancy defects we used the same annihilation rate, $\lambda_L = \lambda_{NV} = 1/\tau_L$, with $\tau_L = 170$ ps. We considered the positron binding energy of the nonvacancy defects of at least 0.3 eV, as these traps were still efficient at 300 K. Since the lifetime spectra decomposition returned only two lifetime components (even when three components decomposition was tested) and we do not observe strong variations of the τ_2 lifetime, we suppose that the lifetimes of the neutral and negative vacancies are indistinguishable. We considered $\tau = 310$ ps for both of them. As for the trapping coefficients, we used $\mu_V = 1 \times 10^{15}$ s^{-1} for the neutral vacancies, $\mu_{V^-} = 4 \times 10^{16}$ s^{-1} at 20 K for the negative vacancies and $\mu_{NV} = 4 \times 10^{16}$ s^{-1} at 20 K for the nonvacancy defects. The choice of the trapping coefficients

was based on the values gathered in Ref. [31] and the predicted charge states of the negative defects.

The fits presented in Fig. 1 were obtained using concentrations $c_V = 6.5 \times 10^{19}$ cm^{-3}, $c_{V^-} = 2 \times 10^{18}$ cm^{-3}, and $c_{NV} = 1 \times 10^{19}$ cm^{-3}. It is worth noting that some of the parameters used in the trapping model were only estimated, hence the absolute values of the concentrations cannot be considered certain. However, conclusions can be drawn on the proportions between the defects concentrations. The best fits of the present experimental data were obtained for the neutral vacancies concentration c_V at least 30 times larger than c_{V^-} and over six times larger than c_{NV}, which suggests that the neutral vacancies are the predominant positron traps in the examined UO_2 samples. Smaller, but not negligible, concentrations of negative nonvacancy defects and vacancies are also present in the material.

V. CALCULATION RESULTS

We performed positron lifetime calculations for several fully relaxed defects in UO_2 containing from one to six vacancies in both GGGC + GC and PSN + GC schemes. The results are presented in Table II. For almost all types of defects, we considered two charge states. First, we performed positron lifetime calculations for neutral defects. Second, we calculated the lifetimes for vacancies in the charge states that were determined as the most stable ones in the stoichiometric material [21,22]. Considering the oxygen vacancy, its formal charge (2+) cannot be detected by PAS. The 2− charge, however, was found to be stable for Fermi levels lying close to the middle of the band gap [21,22], so we studied it as well.

As can be seen in Table II, the differences between the positron lifetimes obtained in the two calculation schemes are lower than 10 ps for almost all considered defects. The biggest differences are found for two large defects, the neutral $2V_U + 2V_O$ tetravacancy (difference of 15 ps) and the 2− charged $2V_U + 4V_O$ hexavacancy (difference of 24 ps). It is also worth noting that similar results are yielded by the PSN + GC and GGGC + GC schemes for the stable charge states of the defects up to the $2V_U$ divacancy, i.e., defects which can most likely be observed in the PAS measurements.

TABLE II. Positron lifetimes calculated in GGGC + GC and PSN + GC schemes for fully relaxed neutral and charged defects in UO_2. The lifetimes obtained for the most stable charge state of each defects are marked in bold.

	Charge	Lifetime GGGC + GC (ps)	Lifetime PSN + GC (ps)
Lattice		168	167
V_O	0	206	199
V_O	2−	203	195
V_U	0	295	304
V_U	4−	**289**	**293**
$V_U + V_O$	0	303	306
$V_U + V_O$	2−	**299**	**301**
$V_U + 2V_O(100)$	0	**301**	**304**
$V_U + 2V_O(110)$	0	**310**	**313**
$V_U + 2V_O(111)$	0	**314**	**316**
$2V_U$	0	313	318
$2V_U$	8−	**290**	**289**
$2V_U + 2V_O$	0	324	339
$2V_U + 2V_O$	4−	**309**	**319**
$2V_U + 4V_O$	0	323	329
$2V_U + 4V_O$	2−	**341**	**365**

For both schemes, we can observe that the lifetimes of the negative defects are almost always shorter than for the neutral ones. It is due to both a smaller relaxation and the higher electronic density in negative defects. However, in the case of the $2V_U + 4V_O$ hexavacancy, the lifetime of the negative charge state is longer than the one of the neutral defect in both calculation schemes. This is due to the fact that the positron is localized in a different way in these two defects. In the GGGC scheme [Figs. 4 (c) and 4(d)], in neutral $2V_U + 4V_O$, the positron is localized inside one of the uranium vacancies, while in 2− charged $2V_U + 4V_O$ the majority of its density can be found between two V_U. In the PSN scheme [Figs. 5 (c) and 5(d)], we find a similar localization between two uranium vacancies in 2− charged $2V_U + 4V_O$. In the case of the neutral hexavacancy, however, the positron density has two maxima, in both uranium vacancies.

In both schemes, it can be observed in several instances that different defects have similar positron lifetimes. For example, in GGGC + GC, the uranium monovacancy V_U^{4-} and divacancy $2V_U^{8-}$ have lifetimes of 289 and 290 ps, respectively. The PSN + GC scheme yields lifetimes of 293 and 289 ps, respectively. The lifetimes obtained for the $(V_U + V_O)^{2-}$ divacancy, 299 ps in GGGC + GC and 301 ps in PSN + GC, are also close to these values. Moreover, using the two methods we calculated positron lifetimes between 301 and 316 ps for the three configurations of the $V_U + 2V_O$ trivacancy and lifetimes of 309 ps (GGGC + GC) and 319 ps (PSN + SC) for $(2V_U + 2V_O)^{4-}$. This can lead to difficulties in the defect identification in the positron annihilation spectroscopy studies.

To understand why different defects have similar positron lifetimes, we plotted the isodensities of the positron localized in these systems. We plot the results obtained in the GGGC + GC scheme in Figs. 2 and 4 and in the PSN + GC scheme in Figs. 3 and 5. It is worth noting that in the PSN + GC scheme we applied the gradient correction on the enhancement factor only, hence there is no effect of this correction on the calculated densities.

First, we can observe that for all defects the GGGC + GC scheme yields more localized positron densities than the PSN scheme, which was expected [45,47]. In all defects presented in Figs. 2 and 4, except the negative hexavacancy, the GGGC scheme finds the positron localized inside one uranium vacancy. In these defects, the positron density is only slightly affected by the presence of the other vacancies. The fact that the positron "senses" similar volumes and geometries in these defects explains why similar lifetimes are obtained in these cases. The $(2V_U + 4V_O)^{2-}$ hexavacancy is the only defect in which the positron localizes between the two uranium vacancies. It is reflected in the longer lifetime of 341 ps calculated for this cluster in the GGGC + GC scheme.

In the PSN scheme, however, we obtain a different positron localization for the clusters containing two uranium vacancies (see Fig. 5). In $(2V_U)^{8-}$ and $(2V_U + 4V_O)^{2-}$ the positron is

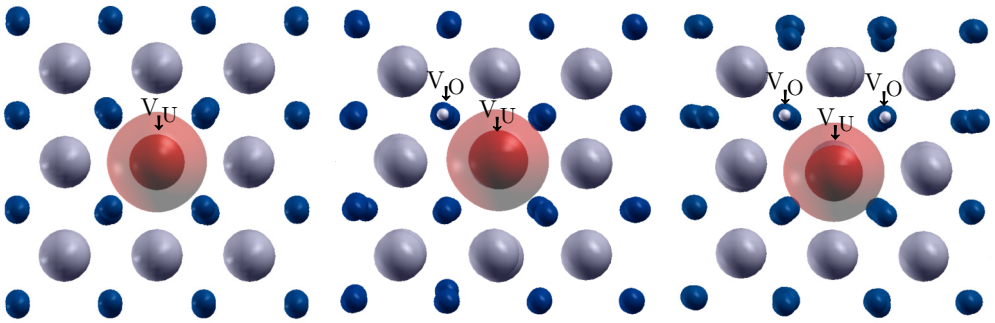

(a) $(V_U)^{4-}$ (b) $(V_U{+}V_O)^{2-}$ (c) $(V_U{+}2V_O)^0(110)$

FIG. 2. (Color online) Positron isodensities found in the GGGC + GC scheme (70% of the maximum density—solid, and 30%—transparent), in red, in the neutral defects containing one uranium vacancy. Uranium atoms are presented in gray, oxygen atoms in blue. White spheres represent the oxygen vacancies. Figures were generated using the XCRYSDEN [65,66] program.

localized between the two uranium vacancies. However, in the 2− charged hexavacancy the free volume that the positron occupies is much larger than in $(2V_U)^{8-}$, hence we observe a significantly longer lifetime for this defect. In both $(2V_U + 2V_O)^{4-}$ and $(2V_U + 4V_O)^0$ defects, we observe two maxima of the positron density, one in each uranium vacancy.

Even though the positron densities yielded by GGGC + GC and PSN + GC differ strongly, using both schemes we obtain very similar positron lifetimes, which are the characteristics that we compare with experiments in the present study. Beside this annihilation characteristic, the momentum distribution of electron-positron pairs can be measured through the Doppler broadening of the annihilation line using a Dopper broadening spectrometer [67]. This distribution is also a valuable source of information on the nature and chemical environment of vacancy defects and is complementary to the lifetime. Especially, the annihilation rate with core electrons is more sensitive to the positron distribution in the defect, hence it should be more affected by the choice of the calculation scheme. Since we are not able to calculate the Doppler broadening yet, we compare the ratio of the core annihilation fractions deduced from the core annihilation rate λ_c as proposed by Puska *et al.* [47] using the expression

$$R_c = \frac{(\lambda_c/\lambda)^{\text{Defect}}}{(\lambda_c/\lambda)^{\text{Lattice}}}, \tag{7}$$

where λ is the total annihilation rate. The R_c parameters calculated for several defects in UO_2 in their most stable charge states are presented in Table III. It is worth noting that the relative R_c parameter depends on the choice of the core and valence electrons in the PAW data set and it will not always correspond to the core annihilation parameter W obtained through the Doppler broadening measurements or calculations. From Table III, we can observe that the GGGC + GC scheme yields R_c values at least twice as small as the PSN + GC scheme does. It is consistent with the results obtained by Puska *et al.*, who for instance observed that the GGGC scheme yielded values of the relative core annihilation fraction parameter (referred to as the estimated W parameter in their work) too small by a factor of two for the Ga vacancy in GaAs, when compared with the measured W parameter. We conclude, therefore, that even tough the lifetimes obtained using the two calculation schemes for the majority of defects in UO_2 are similar, the PSN method should be used in the future calculations of Doppler broadening in this material.

VI. DISCUSSION

In this section, we combine the calculation and experimental results to interpret the signals observed by PAS in the UO_2 samples in the present and previous studies. The

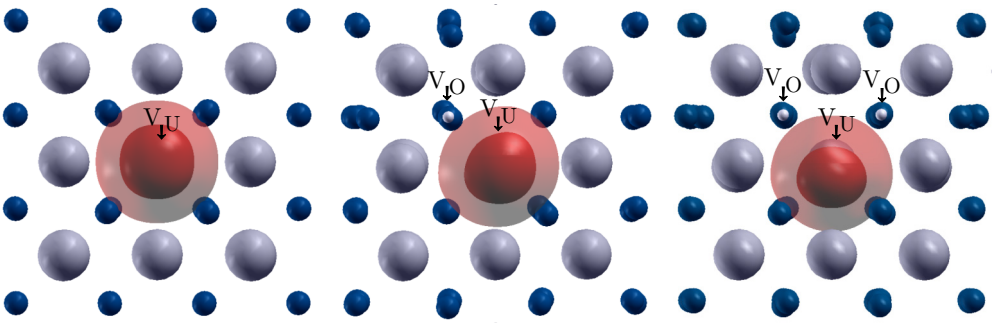

(a) $(V_U)^{4-}$ (b) $(V_U{+}V_O)^{2-}$ (c) $(V_U{+}2V_O)^0(110)$

FIG. 3. (Color online) Positron isodensities found in the PSN + GC scheme (70% of the maximum density—solid, and 30%—transparent), in red, in the neutral defects containing one uranium vacancy. Uranium atoms are presented in gray, oxygen atoms in blue. White spheres represent the oxygen vacancies. Figures were generated using the XCRYSDEN[65,66] program.

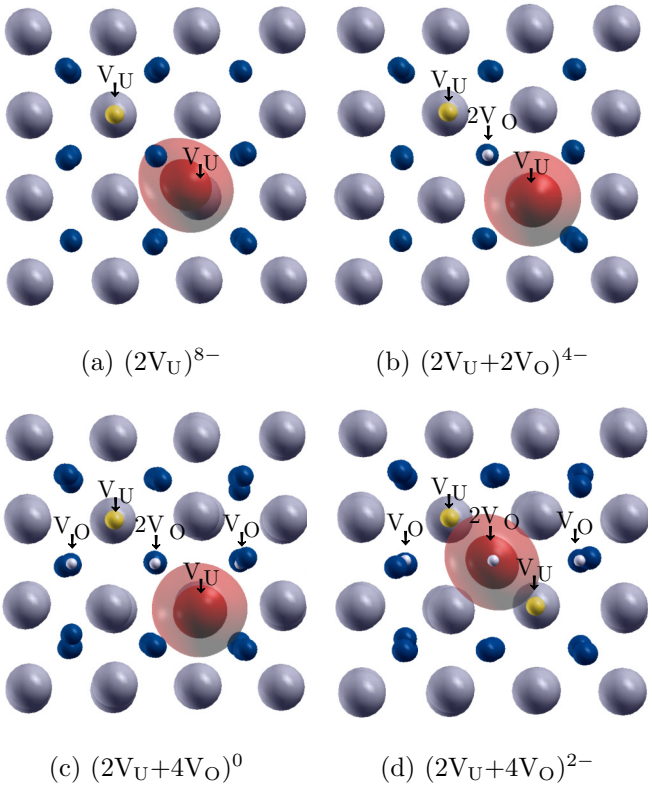

FIG. 4. (Color online) Positron isodensities found in the GGGC + GC scheme (70% of the maximum density—solid, and 30%—transparent), in red, in the neutral defects containing two uranium vacancies. Uranium atoms are presented in gray, oxygen atoms in blue. White and yellow spheres represent oxygen and uranium vacancies, respectively. Figures were generated using the XCRYSDEN [65,66] program.

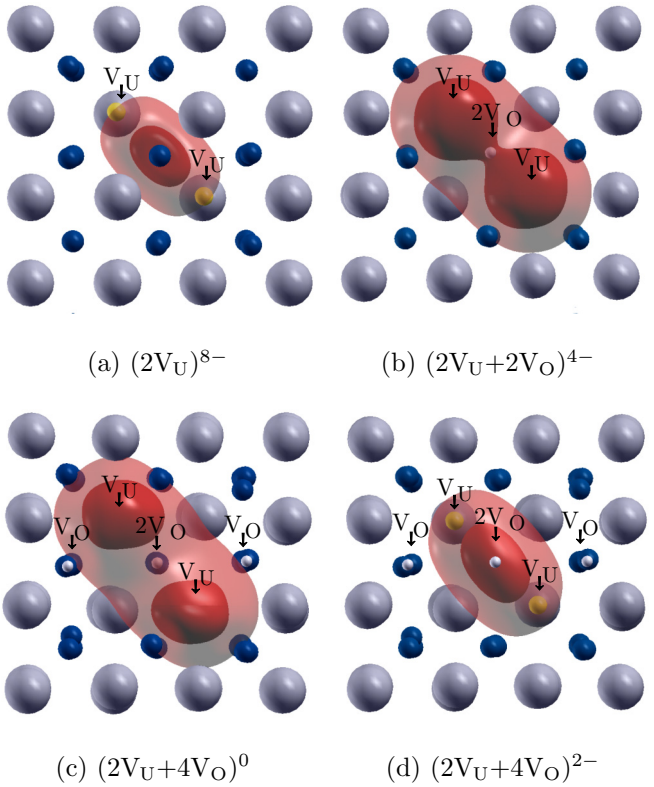

FIG. 5. (Color online) Positron isodensities found in the PSN + GC scheme (70% of the maximum density—solid and 30%—transparent), in red, in the neutral defects containing two uranium vacancies. Uranium atoms are presented in gray, oxygen atoms in blue. White and yellow spheres represent oxygen and uranium vacancies, respectively. Figures were generated using the XCRYSDEN [65,66] program.

short-lifetime component τ_1 detected in the studied UO_2 disks remains close to the experimental lattice lifetime of UO_2 of 170 ± 5 ps for all measurement temperatures (see Fig. 1). This suggests that part of the positrons annihilate around negative nonvacancy defects in the samples. The samples analyzed in this study were slightly hyper-stoichiometric with O/U = 2.0051 ± 0.0001, which means that excess oxygen atoms were already present in the lattice before the α irradiation. The nature of the point defects in the slightly hyperstoichiometric UO_{2+x} structure and their local configurations have been the object of extensive studies, both experimental [1,4,68,69] and theoretical [13–15,20,22,70,71]. Depending on the study, different types of defects containing additional oxygen atoms, such as monointerstitials, di-interstitials, split-interstitials or Willis clusters, are proposed as the most stable ones. All these possible defects structures were found to be stable in negative charge states due to the oxygen ions formal charge state of −2. Recently, Wang *et al.* [71] suggested that the average structure of UO_{2+x} can be represented as a combination of all of these defects structures. Therefore we suppose that the short-lifetime component detected in the studied samples corresponds to mixed signals coming from the positron annihilation around monointerstitials and interstitial clusters charged negatively. These could be defects already present in the unirradiated UO_2 discs or created by irradiation.

The long-lifetime component of 310 ± 5 ps detected in the samples is close to what we calculated for the neutral $V_U + 2V_O$ trivacancy (301–314 ps in GGGC + GC and 304–316 ps in PSN + GC, depending on the configuration) and the $2V_U + 2V_O$ with the −4 charge state (309 ps in GGGC + GC and 319 ps in PSN + GC). The analysis of the evolution of the positron annihilation characteristics as a function of

TABLE III. Relative core annihilation fraction parameter R_c [see Eq. (7)] calculated in the GGGC + GC and PSN + GC schemes for the most stable charge states of defects in UO_2. We also include the result obtained for the neutral oxygen monovacancy.

	Charge	R_c GGGC + GC	R_c PSN + GC
V_O	0	0.39	0.80
V_U	4−	0.23	0.53
$V_U + V_O$	2−	0.23	0.54
$V_U + 2V_O(100)$	0	0.23	0.55
$V_U + 2V_O(110)$	0	0.22	0.55
$V_U + 2V_O(111)$	0	0.22	0.55
$2V_U$	8−	0.26	0.56
$2V_U + 2V_O$	4−	0.23	0.58
$2V_U + 4V_O$	2−	0.09	0.46

the measurement temperature based on the trapping model indicates that two types of vacancy defects are present in the sample, the neutral one being predominant. Theoretical studies on the charge states of the defects clusters in UO_2[14,21,22] suggest that the only neutral defect in the material close to the stoichiometry for the Fermi level near the middle of the band gap is the $V_U + 2V_O$ trivacancy. We propose, hence, that the bound Schottky defects are the neutral vacancies observed in the samples. The analysis of the experimental data based on the positron trapping model implies that negative vacancies are also detected in the UO_2 samples. They should have a positron lifetime close to 310 ps, since only one long component was obtained from the lifetime spectra decompositions. The formation energy calculations of defects in UO_2 [22] suggest that several types of negatively charged vacancies can be present in the material. The positron lifetime calculations presented in this work yield values slightly shorter or longer than 310 ps for various negative defects (from 293 ps for V_U^{4-} to 319 ps for $2V_U + 2V_O$ with the -4 charge state in the PSN + GC scheme). We suppose, hence, that negative uranium monovacancies, U-O divacancies, and $2V_U + 2V_O$ tetravacancies are present in the examined samples. However, the concentration of all these defects are much smaller than the concentration of the Schottky defects.

Our results can be compared with the classical molecular dynamics (CMD) study on 10 keV displacement cascades in UO_2 by Martin *et al.* [23]. The authors found that even though initially mostly monovacancies and monointerstitials were created, they quickly started to form stoichiometric clusters, such as bound Schottky defects, because of the high oxygen mobility. It is worth noting that the empirical potentials used in this study favored the neutral defects over the charged ones and the simulations corresponded to a physical time of approximately 25 ps. Nevertheless, the present results confirm the general conclusion of the CMD study.

In addition to the studies on positron lifetimes in UO_2, measurements of the Doppler broadening of annihilation radiation have also been performed [6–11]. Calculations of the momentum distribution spectra for various defects in UO_2 and their comparison with the experimental data could also bring additional information on the defects in this material. To achieve this goal, we are currently implementing the method allowing the calculation of this annihilation characteristic in the ABINIT code. Since the Doppler broadening is more sensitive to the positron distribution in the defect and the defects configuration, it is worth keeping in mind that the PSN scheme, with a better description of the positron localization, should be more suitable for the modeling of the experimental spectra. Additionally, we observed that the two calculation schemes yield different positron lifetimes for large defects. In the present study we did not observe lifetimes longer than 310 ± 5 ps, however, if larger vacancy clusters are present in UO_2 in future PAS measurements, the choice of the calculation method can affect their identification.

VII. CONCLUSIONS

We performed PAS measurements in UO_2 sintered disks irradiated with 45 MeV α particles at a fluence of 2×10^{16} cm^{-2}. The positron lifetime was measured as function of temperature in the 15–300 K range. We observed two lifetime components, τ_1 of 170 ± 5 ps and τ_2 of 310 ± 5 ps. The short-lifetime component is close to the lattice lifetime for all measurement temperatures. It means that all positrons annihilated in vacancy defects or around negative nonvacancy defects. These nonvacancy defects are assumed to be negative oxygen monointerstitials and interstitials clusters. We used a positron trapping model with three types of positron traps to analyze the evolution of the positron annihilation characteristics in function of measurement temperature. We concluded that a neutral vacancy was the most predominant positron trap, while smaller, but not negligible concentrations of negative vacancies were also present in the material.

We calculated the positron lifetimes of neutral and charged fully relaxed vacancies and vacancy clusters in UO_2 using two different fully self-consistent calculation schemes (GGGC + GC and PSN + GC), in the DFT + U formalism. We observed that the parameters used in the electronic calculations do not affect directly the positron lifetime. However, since the positron lifetime is highly sensitive to the free volume, there is an effect of the equilibrium volume corresponding to the method and the parameters used on the lifetimes obtained. We showed that the gradient correction better describes the absolute values of the positron lifetimes in this material. We showed that the PSN and GGGC schemes yielded similar positron lifetime for the majority of studied defects, especially for the stable charge states of defects up to trivacancies. Therefore similar general conclusions could be drawn by comparing results obtained using both schemes with the experimental values. However, the choice of the calculations scheme could affect the experiments interpretation if larger defects are present in the material.

For several defects, in particular, 2− charged $V_U + V_O$, neutral $V_U + 2V_O$ and 4− charged $2V_U + 2V_O$, we calculated similar positron lifetimes. It is due to the fact that for almost all the studied vacancy clusters the positron is localized in one uranium vacancy and is only slightly affected by the presence of the oxygen vacancies or of the second uranium vacancy. The only cluster having a significantly longer positron lifetime (341 ps) is the 2− charged $2V_U + 4V_O$ hexavacancy, where the positron is localized between the two uranium vacancies.

Comparison of the results obtained experimentally with the calculated positron lifetimes and the most stable charge states of the defects in UO_2 allowed us to identify the predominant neutral vacancy as the $V_U + 2V_O$ trivacancy (bound Schottky defect). This result can be further confirmed by calculations of the momentum distribution spectra for various defects in UO_2 and their comparison with the experimental data. Nevertheless, the present study shows that the coupling of a precise experimental work and calculations using carefully chosen assumptions is an effective method to bring further insight into the defects created by irradiation in UO_2.

ACKNOWLEDGMENTS

This research was partly supported by the french research program NEEDS. The authors are grateful to Boris Dorado and Philippe Garcia for fruitful discussions.

[1] K. Clausen, W. Hayes, J. E. Macdonald, R. Osborn, and M. T. Hutchings, Phys. Rev. Lett. **52**, 1238 (1984).

[2] G. E. Murch and C. R. A. Catlow, J. Chem. Soc., Faraday Trans. 2 **83**, 1157 (1987).

[3] H. Matzke, J. Chem. Soc. Lond. Faraday Trans. 2 **83**, 1121 (1987).

[4] L. Desgranges, M. Gramond, C. Petot, G. Petot-Ervas, P. Ruello, and B. Saadi, J. Eur. Cera. Soc. **25**, 2683 (2005).

[5] R. Konings and O. Beneš, J. Phys. Chem. Sol. **74**, 653 (2013).

[6] M. F. Barthe, S. Guilbert, H. Labrim, P. Desgardin, T. Sauvage, G. Blondiaux, G. Carlot, P. Garcia, and J. P. Piron, Mater. Sci. Forum **445-446**, 48 (2004).

[7] H. Labrim, M.-F. Barthe, P. Desgardin, T. Sauvage, G. Blondiaux, C. Corbel, and J. Piron, App. Surf. Sci. **252**, 3256 (2006).

[8] M.-F. Barthe, H. Labrim, A. Gentils, P. Desgardin, C. Corbel, S. Esnouf, and J. Piron, Phys. Status Solidi C **4**, 3627 (2007).

[9] H. Labrim, M.-F. Barthe, P. Desgardin, T. Sauvage, C. Corbel, G. Blondiaux, and J. Piron, Nucl. Instrum. Meth. B **261**, 883 (2007).

[10] N. Djourelov, B. Marchand, H. Marinov, N. Moncoffre, Y. Pipon, P. Nédélec, N. Toulhoat, and D. Sillou, J. Nucl. Mater. **432**, 287 (2012).

[11] N. Djourelov, B. Marchand, H. Marinov, N. Moncoffre, Y. Pipon, N. Bérerd, P. Nédélec, L. Raimbault, and T. Epicier, J. Nucl. Mater. **443**, 562 (2013).

[12] D. Roudil, M. F. Barthe, C. Jégou, A. Gavazzi, and F. Vella, J. Nucl. Mater. **420**, 63 (2012).

[13] J.-P. Crocombette, D. Torumba, and A. Chartier, Phys. Rev. B **83**, 184107 (2011).

[14] J.-P. Crocombette, Phys. Rev. B **85**, 144101 (2012).

[15] B. Dorado, G. Jomard, M. Freyss, and M. Bertolus, Phys. Rev. B **82**, 035114 (2010).

[16] B. Dorado, D. A. Andersson, C. R. Stanek, M. Bertolus, B. P. Uberuaga, G. Martin, M. Freyss, and P. Garcia, Phys. Rev. B **86**, 035110 (2012).

[17] B. Dorado, B. Amadon, M. Freyss, and M. Bertolus, Phys. Rev. B **79**, 235125 (2009).

[18] D. A. Andersson, B. P. Uberuaga, P. V. Nerikar, C. Unal, and C. R. Stanek, Phys. Rev. B **84**, 054105 (2011).

[19] P. Nerikar, T. Watanabe, J. S. Tulenko, S. R. Phillpot, and S. B. Sinnott, J. Nucl. Mater. **384**, 61 (2009).

[20] M. Freyss, T. Petit, and J.-P. Crocombette, J. Nucl. Mater. **347**, 44 (2005).

[21] J. Wiktor, E. Vathonne, M. Freyss, G. Jomard, and M. Bertolus, MRS Proc. **1645**, mrsf13 (2014).

[22] E. Vathonne, J. Wiktor, M. Freyss, G. Jomard, and M. Bertolus, J. Phys.: Condens. Matter **26**, 325501 (2014).

[23] G. Martin, P. Garcia, C. Sabathier, L. Van Brutzel, B. Dorado, F. Garrido, and S. Maillard, Phys. Lett. A **374**, 3038 (2010).

[24] M. J. Puska and R. M. Nieminen, Rev. Mod. Phys. **66**, 841 (1994).

[25] R. M. Nieminen, E. Boroński, and L. J. Lantto, Phys. Rev. B **32**, 1377 (1985).

[26] S. Dudarev, D. Manh, and A. Sutton, Philos. Mag. Part B **75**, 613 (1997).

[27] M. Saito and A. Oshiyama, Phys. Rev. B **53**, 7810 (1996).

[28] D. V. Makhov and L. J. Lewis, Phys. Rev. B **71**, 205215 (2005).

[29] I. Makkonen, M. Hakala, and M. J. Puska, Phys. Rev. B **73**, 035103 (2006).

[30] I. Makkonen and M. J. Puska, Phys. Rev. B **76**, 054119 (2007).

[31] F. Tuomisto and I. Makkonen, Rev. Mod. Phys. **85**, 1583 (2013).

[32] J. Wiktor, G. Jomard, M. Torrent, and M. Bertolus, Phys. Rev. B **87**, 235207 (2013).

[33] J. Wiktor, G. Jomard, and M. Bertolus, Nucl. Instrum. Meth. B **327**, 63 (2014).

[34] J. Wiktor, X. Kerbiriou, G. Jomard, S. Esnouf, M.-F. Barthe, and M. Bertolus, Phys. Rev. B **89**, 155203 (2014).

[35] J. Soullard, J. Nucl. Mater. **135**, 190 (1985).

[36] P. Kirkegaard and M. Eldrup, Comput. Phys. Commun. **3**, 240 (1972).

[37] M. J. Puska, C. Corbel, and R. M. Nieminen, Phys. Rev. B **41**, 9980 (1990).

[38] C. Corbel, F. Pierre, K. Saarinen, P. Hautojärvi, and P. Moser, Phys. Rev. B **45**, 3386 (1992).

[39] K. Saarinen, A. P. Seitsonen, P. Hautojärvi, and C. Corbel, Phys. Rev. B **52**, 10932 (1995).

[40] K. Saarinen, T. Laine, S. Kuisma, J. Nissilä, P. Hautojärvi, L. Dobrzynski, J. M. Baranowski, K. Pakula, R. Stepniewski, M. Wojdak, A. Wysmolek, T. Suski, M. Leszczynski, I. Grzegory, and S. Porowski, Phys. Rev. Lett. **79**, 3030 (1997).

[41] R. Krause-Rehberg and H. S. Leipner, *Positron Annihilation in Semiconductors: Defect Studies*, Vol. 127 (Springer, 1999).

[42] A. Zubiaga, F. Plazaola, J. A. García, F. Tuomisto, V. Muñoz Sanjosé, and R. Tena-Zaera, Phys. Rev. B **76**, 085202 (2007).

[43] F. Tuomisto, K. Saarinen, D. C. Look, and G. C. Farlow, Phys. Rev. B **72**, 085206 (2005).

[44] F. Tuomisto, V. Ranki, D. C. Look, and G. C. Farlow, Phys. Rev. B **76**, 165207 (2007).

[45] L. Gilgien, G. Galli, F. Gygi, and R. Car, Phys. Rev. Lett. **72**, 3214 (1994).

[46] E. Boroński and R. M. Nieminen, Phys. Rev. B **34**, 3820 (1986).

[47] M. J. Puska, A. P. Seitsonen, and R. M. Nieminen, Phys. Rev. B **52**, 10947 (1995).

[48] J. Arponen and E. Pajanne, J. Phys. F **9**, 2359 (1979).

[49] M. J. Puska, J. Phys.: Condens. Matter **3**, 3455 (1991).

[50] B. Barbiellini, M. J. Puska, T. Korhonen, A. Harju, T. Torsti, and R. M. Nieminen, Phys. Rev. B **53**, 16201 (1996).

[51] J. Kuriplach and B. Barbiellini, J. Phys.: Conf. Ser. **505**, 012040 (2014).

[52] M. Torrent, F. Jollet, F. Bottin, G. Zérah, and X. Gonze, Comput. Mat. Sci. **42**, 337 (2008), http://www.abinit.org.

[53] X. Gonze, B. Amadon, P.-M. Anglade, J.-M. Beuken, F. Bottin, P. Boulanger, F. Bruneval, D. Caliste, R. Caracas, M. Côté, T. Deutsch, L. Genovese, P. Ghosez, M. Giantomassi, S. Goedecker, D. R. Hamann, P. Hermet, F. Jollet, G. Jomard, S. Leroux, M. Mancini, S. Mazevet, M. J. T. Oliveira, G. Onida, Y. Pouillon, T. Rangel, G.-M. Rignanese, D. Sangalli, R. Shaltaf, M. Torrent, M. J. Verstraete, G. Zerah, and J. W. Zwanziger, Comput. Phys. Commun. **180**, 2582 (2009), http://www.abinit.org.

[54] P. E. Blöchl, Phys. Rev. B **50**, 17953 (1994).

[55] N. A. W. Holzwarth, A. R. Tackett, and G. E. Matthews, Comput. Phys. Commun. **135**, 329 (2001), http://users.wfu.edu/natalie/papers/pwpaw/man.html.

[56] J. P. Perdew, K. Burke, and M. Ernzerhof, Phys. Rev. Lett. **77**, 3865 (1996).

[57] A. I. Liechtenstein, V. I. Anisimov, and J. Zaanen, Phys. Rev. B **52**, R5467 (1995).

[58] A. Kotani and T. Yamazaki, Prog. Theor. Phys. Suppl. **108**, 117 (1992).
[59] H. J. Monkhorst and J. D. Pack, Phys. Rev. B **13**, 5188 (1976).
[60] P. Santini, R. Lémanski, and P. Erdős, Adv. Phys. **48**, 537 (1999).
[61] P. Santini, S. Carretta, G. Amoretti, R. Caciuffo, N. Magnani, and G. H. Lander, Rev. Mod. Phys. **81**, 807 (2009).
[62] B. Dorado and P. Garcia, Phys. Rev. B **87**, 195139 (2013).
[63] J. Schoenes, J. Appl. Phys. **49**, 1463 (1978).
[64] M. Idiri, T. Le Bihan, S. Heathman, and J. Rebizant, Phys. Rev. B **70**, 014113 (2004).
[65] A. Kokalj, J. Mol. Graph. Model. **17**, 176 (1999).
[66] A. Kokalj, Comput. Mat. Sci. **28**, 155 (2003).
[67] M. Alatalo, H. Kauppinen, K. Saarinen, M. J. Puska, J. Mäkinen, P. Hautojärvi and R. M. Nieminen, Phys. Rev. B **51**, 4176 (1995).
[68] G. C. Allen, P. M. Tucker, and J. W. Tyler, J. Phys. Chem. **86**, 224 (1982).
[69] G. C. Allen and P. A. Tempest, Proc. R. Soc. Lond. A **406**, 325 (1986).
[70] B. T. M. Willis, Acta Cristallogr. A **34**, 88 (1978).
[71] J. Wang, R. C. Ewing, and U. Becker, Sci. Rep. **4**, 4216 (2014).